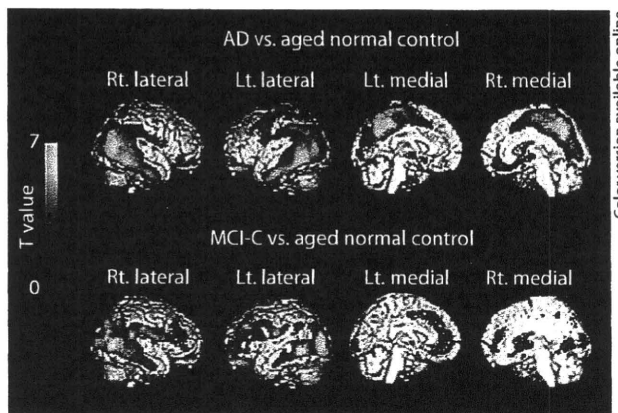


discriminate among groups was assessed using receiver operating characteristic (ROC) analysis. The area under the ROC curve (AUC) and SE were calculated and compared using GraphPad Prism software (GraphPad, San Diego, Calif., USA). Correlations between stainability of A $\beta$  immunostaining and BF-227 staining were examined using the nonparametric Spearman rank correlation analysis. The paired t test was used to examine the difference in cored plaque density between the frontal and temporal cortices. Statistical significance for each analysis was defined as  $p < 0.05$ . These analyses were performed using GraphPad Prism software.

## Results

A statistically significant difference in age between aged normal controls and patients with MCI ( $p < 0.05$ ) was observed. However, no statistically significant difference in age between MCI-C and MCI-NC as well as between aged normal controls and patients with AD was observed. Patients with AD showed a significantly lower MMSE score than aged normal controls. In addition, the AD2 group showed a significantly lower MMSE score than the MCI-NC group. However, no statistically significant difference in MMSE score was observed among other groups.

Voxel-based analysis of [ $^{11}\text{C}$ ]BF-227 PET images demonstrated that MCI-C and patients with AD had significantly higher [ $^{11}\text{C}$ ]BF-227 uptake in the neocortical region than aged normal controls (fig. 1; tables 2, 3). Bilateral temporoparietal BF-227 uptake was evident in both the AD and MCI-C groups although significant uptake in the posterior cingulate cortex and precuneus was observed only in the AD group. In the AD and MCI-C groups, the difference in the lateral frontal cortex was less evident compared with that in the lateral temporoparietal region. In contrast to the MCI-C group, the MCI-NC group showed no significant elevation of BF-227 uptake compared with the aged normal control group. Z-score maps of PET images were created by comparison with the normal control database (fig. 2). Most patients with AD showed a Z-score greater than 2 in the bilateral temporal and posterior cingulate cortices. In contrast, 10 out of the 12 aged normal controls (83%) showed no remarkable change in neocortical BF-227 uptake, except for 2 subjects (17%) showing modest changes in the lateral temporal and cingulate cortices. MCI-C tended to show higher neocortical Z-scores than MCI-NC (fig. 2b). Among the 7 MCI-C, 4 showed BF-227 uptake in the bilateral temporoparietal and frontal cortices, while the other 2 showed moderate abnormality in the temporal and frontal Z-scores. In MCI-C, changes in BF-227 uptake within the



**Fig. 1.** Brain regions showing significantly higher uptake of [ $^{11}\text{C}$ ]BF-227 in patients with AD (upper images) and MCI-C (lower images) compared with data from aged normal controls ( $p < 0.05$ , corrected for multiple comparisons). The red-to-yellow scale indicates the level of statistical significance of the differences in [ $^{11}\text{C}$ ]BF-227 uptake (yellow: most significant difference).

posterior cingulate cortex were relatively moderate compared with those in the lateral temporal cortex. One MCI-C showed limited change in BF-227 uptake within the temporal cortex and precuneus. In contrast to MCI-C, most MCI-NC showed no abnormal BF-227 uptake in the lateral temporal cortex, except for 1 who showed a slightly higher Z-score in the temporal cortex and an extremely high score in the posterior cingulate cortex. Another 3 MCI-NC also showed limited abnormality in the posterior cingulate cortex and precuneus but no abnormal Z-score in the lateral temporal cortex. No significant difference in BF-227 uptake was observed between the MCI-NC and MCI-C groups, MCI-NC and AD groups, and MCI-C and AD groups. Furthermore, no significant region showing reduction in BF-227 uptake in the MCI and AD groups compared with the aged normal controls was observed.

ROI analysis data were roughly consistent with voxel-based analysis data (fig. 3; table 4). The MCI-C group showed higher retention of [ $^{11}\text{C}$ ]BF-227 in the frontal, temporal and parietal cortices than the aged normal control group. The AD1 group showed higher BF-227 retention in the frontal, temporal, parietal and occipital cortices than the aged normal control group. The AD2 group showed higher BF-227 retention in the temporal, parietal, occipital and posterior cingulate cortices than the aged normal control group, with the exception of the frontal cortex. Furthermore, significantly higher BF-227 uptake

**Table 2.** Talairach coordinates of within-cluster peak areas showing significantly higher BF-227 uptake in AD patients compared with aged normal group ( $p < 0.05$ , false discovery rate corrected)

k	T value	Talairach coordinates			Region
		x	y	z	
48,058	7.15 (5.38)	54	-46	-12	right inferior temporal gyrus
	6.79 (5.21)	50	-62	14	right middle temporal gyrus
	6.22 (4.92)	-52	-58	-2	left middle temporal gyrus
760	4.81 (4.09)	-24	4	-4	left putamen

Values in parentheses denote Z values.

**Table 3.** Talairach coordinates of within-cluster peak areas showing significantly higher BF-227 uptake in MCI-C compared with aged normal group ( $p < 0.05$ , false discovery rate corrected)

k	T value	Talairach coordinates			Region
		x	y	z	
14,893	6.19 (4.42)	46	-64	6	right middle temporal gyrus
	5.84 (4.27)	40	-74	14	right middle temporal gyrus
	5.52 (4.12)	52	-44	-8	right temporal lobe subgyrus
6,768	5.78 (4.24)	-36	32	34	left middle frontal gyrus
	4.78 (3.75)	-58	-16	24	left parietal lobe
	4.70 (3.71)	-24	50	0	left superior frontal gyrus
5,893	5.77 (4.24)	-38	-80	10	left middle occipital gyrus
	5.52 (4.12)	-42	-60	-4	left middle temporal gyrus
	5.27 (4.00)	-22	-92	-4	left cuneus

Values in parentheses denote Z values.

was found in the frontal and temporal cortices of the MCI-C group as well as in the temporal and parietal cortices of the AD group compared with the MCI-NC group. Compared with the AD group, Cohen's  $d$  was higher in the temporal (2.93) and parietal (2.25) cortices than in the frontal (1.69) and posterior cingulate (1.51) cortices for the aged normal control group. When comparing the MCI-C and MCI-NC groups, the highest Cohen's  $d$  was observed in the temporal (1.70) and parietal (1.76) cortices, followed by the frontal (1.62), posterior cingulate (0.85) and occipital (0.37) cortices, indicating that the difference in SUVR is the largest in the temporoparietal cortex when comparing the MCI-C and MCI-NC groups. Furthermore, ROC analysis demonstrated higher AUC values with the temporal SUVR ( $AUC = 0.987$ ;  $SE = 0.016$ ) than with the frontal SUVR ( $AUC = 0.915$ ;  $SE = 0.052$ ) for the discrimination between the AD and aged normal control groups as well as between the MCI-C and MCI-

NC groups (fig. 4). Using the temporal BF-227 SUVR of 1.10 (1.5 SD above control mean) as the cutoff, a sensitivity of 95% and specificity of 92% in the discrimination between AD and aged normal groups, and a sensitivity of 100% and specificity of 57% in the discrimination between MCI-C and MCI-NC was achieved.

To explain why BF-227 preferentially accumulates in the temporal cortex as opposed to the frontal cortex of the AD brain, we examined the binding characteristics of BF-227 to  $A\beta$  deposits, using postmortem AD brain samples. BF-227 showed good stainability for dense-type plaques in the frontal and temporal cortices. Diffuse plaques in the frontal cortex tended to be larger than those in the temporal cortex. However, the stainability for diffuse-type plaques in the frontal cortex was relatively weaker than that in the temporal cortex (fig. 5). The mean number of  $A\beta$  plaques positively stained with BF-227 was significantly higher in the temporal cortex than in the fron-

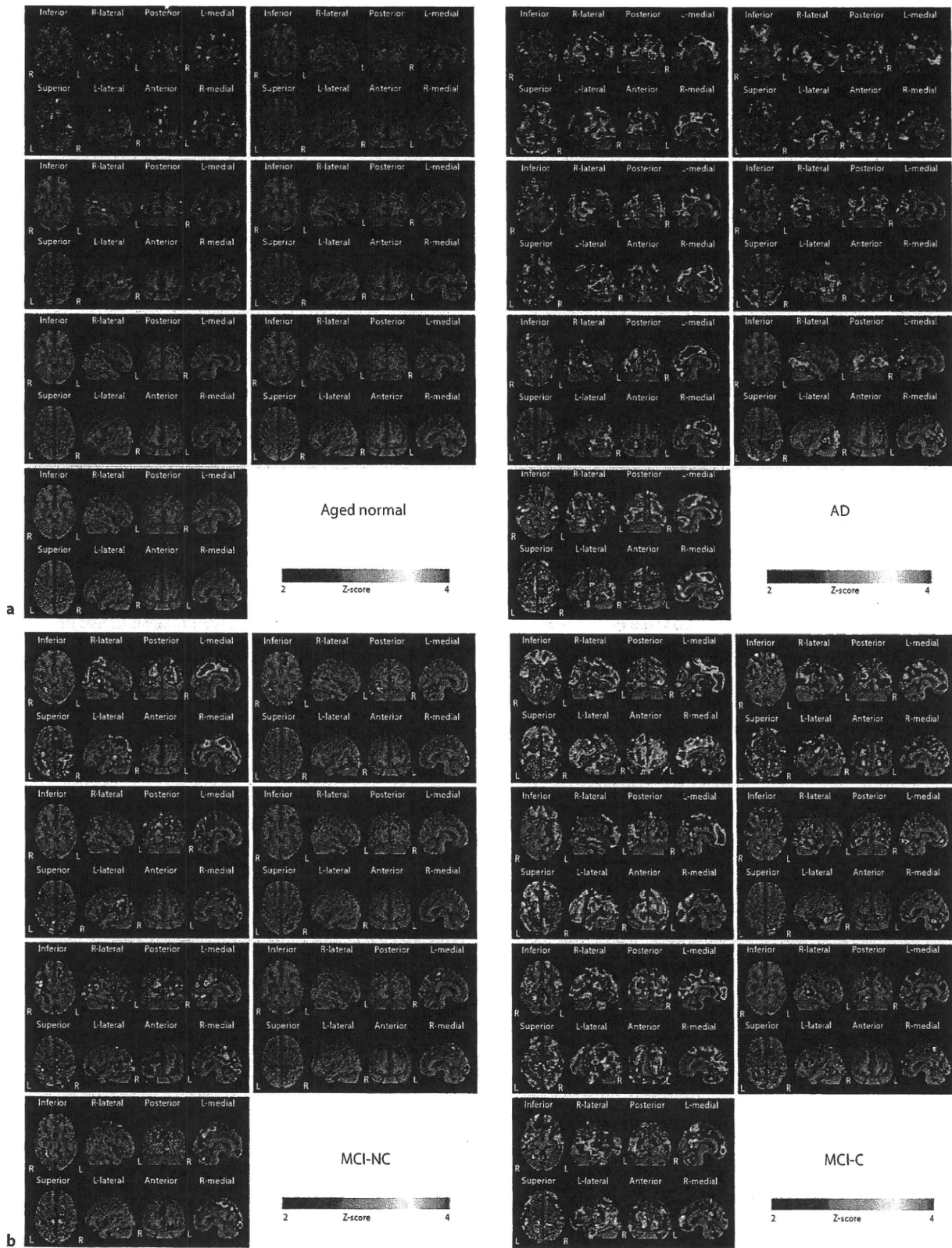


**Table 4.** Average SUVR between 20 and 40 min after injection

	SUVR					Cohen's d	
	aged normal	MCI-NC	MCI-C	AD1	AD2	MCI-NC and MCI-C	aged normal and all AD
Frontal	0.98 ± 0.05	0.98 ± 0.06	1.11 ± 0.10* <sup>#</sup>	1.08 ± 0.08*	1.06 ± 0.05	1.62	1.69
Temporal	1.02 ± 0.04	1.06 ± 0.07	1.18 ± 0.07* <sup>#</sup>	1.18 ± 0.07* <sup>#</sup>	1.18 ± 0.06* <sup>#</sup>	1.7	2.93
Parietal	1.06 ± 0.04	1.08 ± 0.05	1.17 ± 0.05*	1.18 ± 0.06* <sup>#</sup>	1.19 ± 0.09*	1.76	2.25
Occipital	1.05 ± 0.04	1.09 ± 0.06	1.11 ± 0.06	1.13 ± 0.07*	1.13 ± 0.05*	0.37	1.51
Posterior cingulate	1.11 ± 0.07	1.12 ± 0.07	1.19 ± 0.10	1.20 ± 0.09	1.22 ± 0.05*	0.85	1.51

Values denote means ± SD. \*  $p < 0.05$  versus aged normal group; <sup>#</sup>  $p < 0.05$  versus MCI-NC group.

tal cortex. In the temporal cortex, the number of positively stained A $\beta$  plaques showed a significantly positive correlation with the number of dense- and diffuse-type plaques. However, in the frontal cortex, the number of positively stained A $\beta$  plaques showed a significant correlation with only the number of dense-type plaques and not with the number of diffuse-type plaques (fig. 6).

## Discussion

The identification of patients with a high risk of developing AD in the MCI stage is of great clinical value. However, it is difficult to predict the conversion from MCI to AD from a clinical and neuropsychological perspective. In comparison with MRI and CT, PET is relatively expensive and not accessible. Consequently, PET is not routinely used in the diagnosis of AD. However, PET imaging provides useful diagnostic information for predicting conversion from MCI to AD when MRI fails to provide sufficient information [15]. A recent Pittsburgh compound B (PiB) PET study demonstrated that in vivo detection of amyloid deposition provides useful prognostic information in MCI [19]. The present study using BF-227

PET showed similar predictive performance to previous PiB PET results although the signal-to-background ratio increase for BF-227 in patients with AD over controls was considerably lower than that for PiB. The lower signal-to-background ratio of BF-227 would be due to the lower detection sensitivity of BF-227 than that of PiB for diffuse plaques. However, BF-227 PET may have a better predictive value for progression from MCI to AD than PiB PET because the deposition of diffuse plaque is observed even during the normal aging process. A head-to-head comparison of BF-227 PET with PiB PET will clarify which tracer has more predictive power for conversion of MCI to AD.

Voxel-based analysis of PET images allows an objective and sensitive identification of regional change in uptake of the tracer. BF-227 is a PET tracer that binds to amyloid plaques in the brain [10]. Although BF-227 binds well to amyloid fibrils in vitro, the signal-to-background ratio for [<sup>11</sup>C]BF-227 PET images was relatively lower than that for PiB PET, possibly due to the lower binding affinity of BF-227 to A $\beta$  fibrils compared to PiB. This drawback can be overcome by voxel-based statistical comparison with a normal control database. In fact, the abnormal distribution of [<sup>11</sup>C]BF-227 in MCI-C was more clearly demonstrated by Z-score mapping analysis than by unprocessed SUVR images. In addition, a portion of MCI-NC showed a high Z-score in the posterior neocortical areas, which may reflect early A $\beta$  pathology in the brain. The pathological significance of these abnormalities will be elucidated after having followed up these patients.

A commonly observed feature in the Z-score maps of MCI-C and patients with AD was the change in bilateral temporal and temporooccipital cortices, which was also detected by between-group comparison with the aged

**Fig. 2. a** Voxel-by-voxel Z-score analysis of [<sup>11</sup>C]BF-227 PET images for aged normal subjects (left) and patients with AD (right) with the mean and SD of PET images of 15 normal controls. The Z-score maps were displayed by the surface projection of the spatially normalized MR image. **b** Voxel-by-voxel Z-score analysis by comparison of [<sup>11</sup>C]BF-227 PET images for MCI-NC (left) and MCI-C (right) with the mean and SD of PET images of 15 normal controls. The Z-score maps were displayed by the surface projection of the spatially normalized MR image.

**Fig. 3.** Regional BF-227 SUVR in the frontal (a) and temporal (b) cortices. Horizontal bar: average SUVR in each group. \*  $p < 0.05$ .

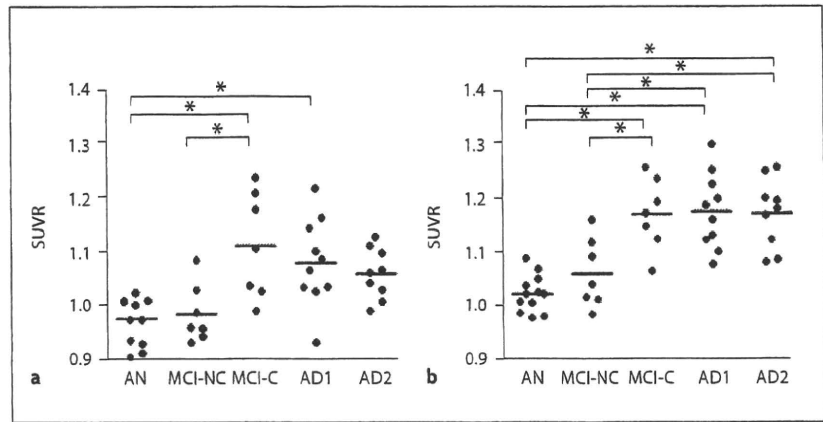


**Fig. 4.** ROC curves of regional BF-227 SUVR in the frontal (a) and temporal (b) cortices for differentiation between patients with AD and aged normal controls (solid line) and between MCI-C and MCI-NC (dashed line).

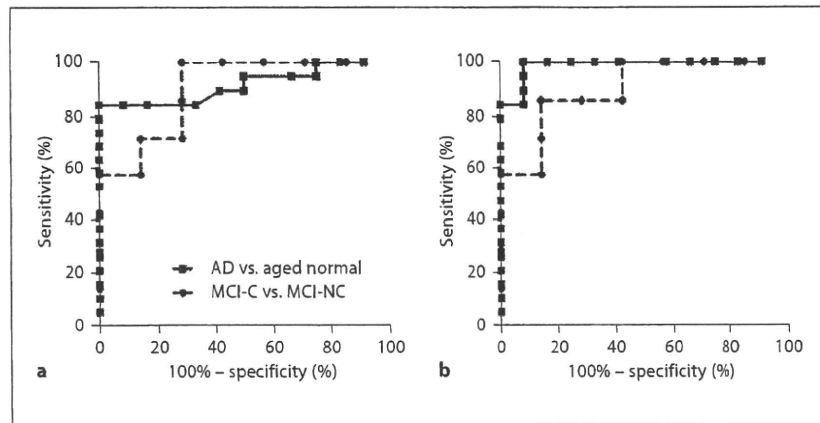
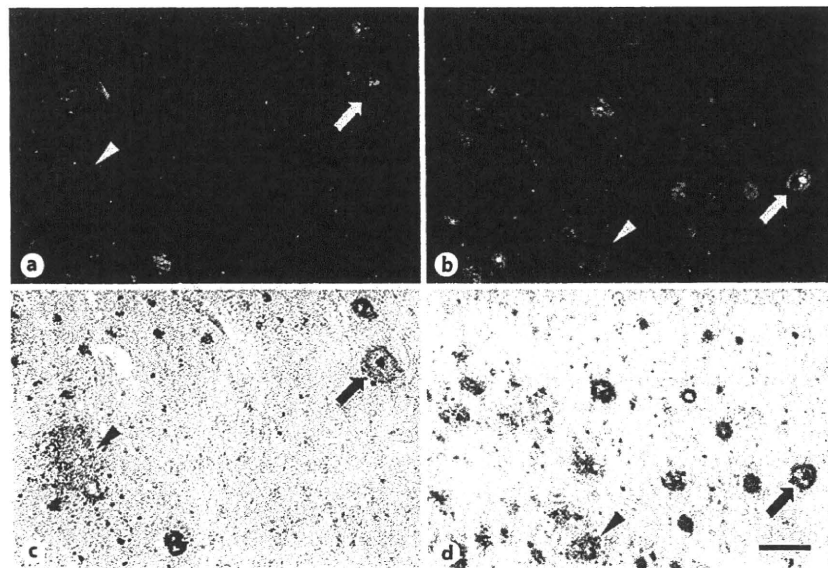


**Fig. 5.** Neuropathologic staining of AD frontal (a, c) and temporal (b, d) brain sections by BF-227. Cored plaques (arrows) are clearly stained with BF-227 (a, b). Cored-plaque staining with BF-227 correlates well with A $\beta$  immunostaining in adjacent sections (c, d). Diffuse plaques (arrowheads) are faintly stained with BF-227 in the frontal brain section (a), but moderately stained in the temporal brain section (b). Scale bar = 100  $\mu$ m.



Color version available online

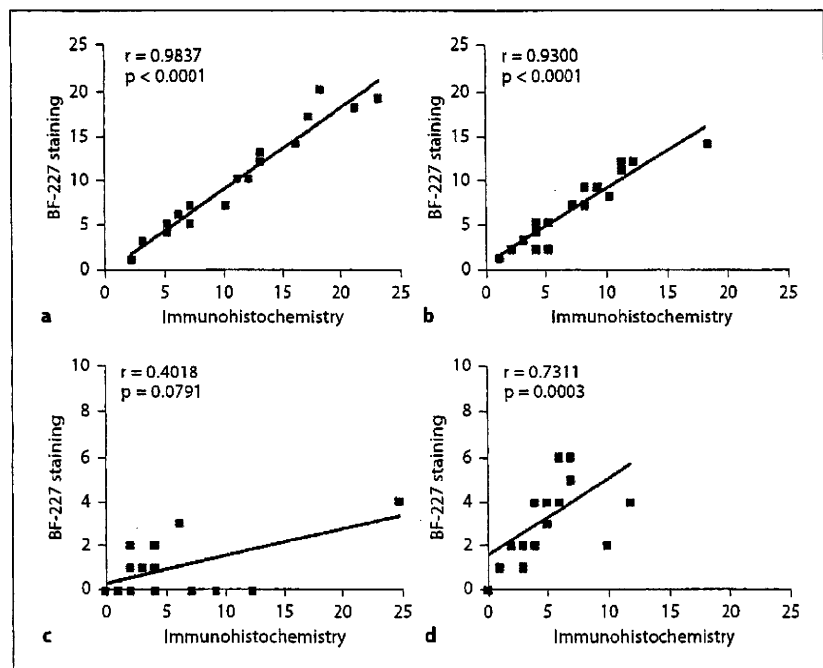


**Fig. 6.** Correlations between the numbers per unit area of amyloid plaques stained with A $\beta$ -specific antibody and BF-227. The density of dense-type plaques showed a significant correlation with positive staining with BF-227 both in the frontal (a) and temporal (b) brain sections. However, the density of diffuse-type plaques was not correlated with BF-227 staining in the frontal cortex (c), and weakly correlated with BF-227 staining in the temporal cortex (d).

normal controls using the SPM software. The preferential [ $^{11}\text{C}$ ]BF-227 retention in the posterior neocortical region corresponded with an area containing a high density of neuritic plaques [20]. This finding was confirmed by our analysis using postmortem AD brain samples. From these findings, the amount of dense plaque deposits in the posterior neocortical region, which could be measured by [ $^{11}\text{C}$ ]BF-227 PET, is a reliable index of prognosis in patients with MCI. Interestingly, the Z-score mapping of BF-227 PET images further elucidated individual variation in the regional distribution of amyloid plaque deposition in patients with AD. There is great interest in determining the relationship between this heterogeneity and the clinical phenotype of patients with AD, which should be investigated in the future with data from a larger population. About 2/3 of patients with AD showed elevated BF-227 uptake in both anterior and posterior association areas, and the remaining 1/3 showed posterior-oriented BF-227 uptake. However, none of the patients with AD showed frontal-oriented BF-227 uptake. Although our analysis has been cross-sectional, these findings suggest that neuritic plaque deposition in AD starts at the posterior association areas and then spreads to other brain regions during AD progression.

The relatively lower [ $^{11}\text{C}$ ]BF-227 retention in the frontal cortex of patients in the AD group may be a chance

finding due to the small sample size. However, previous analysis of postmortem AD brain samples indicated that a majority of neocortical plaques start as fibrillar A $\beta$  deposits and, in the late stages of AD, shift to nonfibrillar plaques [21]. Therefore, the relatively lower [ $^{11}\text{C}$ ]BF-227 uptake in the AD group may be due to the transformation of fibrillar A $\beta$  deposits to nonfibrillar A $\beta$  deposits during AD progression. A longitudinal evaluation of [ $^{11}\text{C}$ ]BF-227 uptake is necessary to examine whether the neocortical A $\beta$  deposits reflected by BF-227 uptake change during the course of AD progression. In addition, the quantitative analysis of BF-227 binding to amyloid plaques should be performed in the future to eliminate the influence of regional cerebral hypoperfusion.

The definitive diagnosis of AD depends on postmortem examination because histological analysis of tissue samples is the only method for assessing AD pathology with certainty [7, 22]. Senile plaques were classified on the basis of the morphology of histopathological staining: diffuse plaques, primitive plaques, classical plaques and compacted plaques [23]. The diffuse plaques were abundant in healthy controls, whereas mature plaques such as primitive, classical and compact ones were typical in patients with AD. In our study, strong correlations between the number of mature plaques and BF-227 binding in the frontal and temporal cortices were observed. Further-

more, the temporal cortex exhibited a significant correlation between the number of diffuse-type plaques and BF-227 binding. However, the frontal cortex showed no such correlation. Generally, primitive, classical and compact plaques contain more amyloid fibrils than diffuse plaques. A previous electron microscopic examination has suggested that diffuse plaques in the frontal cortex contain a small amount of amyloid fibrils and do not easily transform to primitive plaques, while those in the temporal cortex contain more amyloid fibrils and tend to transform to primitive plaques [24]. Therefore, the binding ability of BF-227 to different types of diffuse plaques in the frontal and temporal cortices partly explains why BF-227 tends to accumulate in the temporal cortex of the AD brain. In addition, the density of dense-type plaques in the temporal cortex was higher than that in the frontal cortex in our analysis. This finding is in accordance with another comprehensive neuropathological examination that showed a higher density of amyloid plaques in the temporal cortex than in the frontal cortex [20, 25]. Thus, the lower density of primitive plaques in the frontal cortex may explain the relatively lower BF-227 uptake in the frontal cortex. Further analyses using more AD brain samples and radiolabeled BF-227 are required in the future because only one brain was examined in this study, and the concentration of BF-227 used to stain the post-mortem tissue was not equivalent to the expected *in vivo* concentrations.

Previous PiB PET studies have shown the greatest tracer uptake in the precuneus and posterior cingulate cortex. However, our PET study demonstrated greater BF-227 uptake in the lateral temporal and parietal cortices of the AD brain samples than in the posterior cingulate cortex. A recent study demonstrated that the number of diffuse plaques in the posterior cingulate gyrus was greater than that in other neocortical areas. However, the number of neuritic plaques in the posterior cingulate cortex was not greater than that in other neocortical areas during AD progression [26]. Therefore, the modest posterior cingulate BF-227 uptake elevation in some patients with AD may be due to the lower binding affinity of BF-227 to diffuse plaques than that of PiB.

There are several limitations of this study. First, the sample size was small, primarily because of the limited follow-up period. Second, no repeat scans were performed to really assess changes in BF-227 uptake over time. Future studies should include longitudinal data from a larger sample. Third, the patients with MCI were older than the aged normal controls. Therefore, the higher neocortical uptake of [<sup>11</sup>C]BF-227 in patients with MCI

could be attributed to the effect of aging. However, no age-related change in BF-227 uptake was observed in the aged normal controls [10]. Furthermore, no significant elevation of [<sup>11</sup>C]BF-227 uptake was observed in the MCI-NC group compared with that in the aged normal control group. Therefore, the higher [<sup>11</sup>C]BF-227 uptake in the MCI-C group is not likely due to the effect of aging. We need to further address this issue by controlling for the age of normal controls and patients with MCI.

In summary, [<sup>11</sup>C]BF-227 PET can detect the early A $\beta$  load in the lateral temporal cortex of patients with MCI and AD. The amount of [<sup>11</sup>C]BF-227 uptake in the temporal cortex was strongly related to prognosis in patients with MCI. BF-227 would be less subjective to amyloid pathology during the process of aging since this probe is believed to bind selectively to dense A $\beta$  plaques. Thus, [<sup>11</sup>C]BF-227 PET offers unique information concerning AD pathology that cannot be obtained by other PET tracers, which would be useful for the MCI population since it allows prediction of their risk for progression to AD in the near future.

#### Acknowledgments

This study was supported by the Health and Labor Sciences Research Grants for Translational Research from the Ministry of Health and the Grant-in-Aid for Scientific Research on Priority Areas – Integrative Brain Research from the Ministry of Education, Culture, Sports, Science, and Technology of Japan (20019006). We appreciate the technical assistance provided by Dr. S. Watanuki, Dr. Y. Ishikawa and M. Kato during the PET studies.

#### References

- 1 Glenner GG, Wong CW: Alzheimer's disease: initial report of the purification and characterization of a novel cerebrovascular amyloid protein. *Biochem Biophys Res Commun* 1984;120:885–890.
- 2 Masters CL, Multhaup G, Simms G, Pottgiesser J, Martins RN, Beyreuther K: Neuronal origin of a cerebral amyloid: neurofibrillary tangles of Alzheimer's disease contain the same protein as the amyloid of plaque core and blood vessels. *EMBO J* 1985;4:2757–2763.
- 3 Masters CL, Simms G, Weinman NA, Multhaup G, McDonald BL, Beyreuther K: Amyloid plaque core protein in Alzheimer disease and Down syndrome. *Proc Natl Acad Sci USA* 1985;82:4245–4249.
- 4 Hardy J, Selkoe DJ: The amyloid hypothesis of Alzheimer's disease: progress and problems on the road to therapeutics. *Science* 2002;297:353–356.

- 5 Petersen RC, Smith GE, Waring SC, Ivnik RJ, Tangalos EG, Kokmen E: Mild cognitive impairment: clinical characterization and outcome. *Arch Neurol* 1999;56:303–308.
- 6 Petersen RC: Mild cognitive impairment as a diagnostic entity. *J Intern Med* 2004;256:183–194.
- 7 Ikonomic MD, Klunk WE, Eric E, Abrahamson EE, Mathis CA, Price JC, Tsopelas ND, Lopresti BJ, Ziolkowski S, Bi WZ, Paljug WR, Debnath ML, Hope CE, Barbara A, Isanski BA, Hamilton RL, DeKosky ST: Post-mortem correlates of in vivo PiB-PET amyloid imaging in a typical case of Alzheimer's disease. *Brain* 2008;131:1630–1645.
- 8 Furumoto S, Okamura N, Iwata R, Yanai K, Arai H, Kudo Y: Recent advances in the development of amyloid imaging agents. *Curr Top Med Chem* 2007;7:1773–1789.
- 9 Klunk WE, Engler H, Nordberg A, Wang Y, Blomqvist G, Holt DP, Bergström M, Savitcheva I, Huang GF, Estrada S, Ausén B, Debnath ML, Barletta J, Price JC, Sandell J, Lopresti BJ, Wall A, Koivisto P, Antoni G, Mathis CA, Långström B: Imaging brain amyloid in Alzheimer's disease with Pittsburgh Compound-B. *Ann Neurol* 2004;55:306–319.
- 10 Kudo Y, Okamura N, Furumoto S, Tashiro M, Furukawa K, Maruyama M, Itoh M, Iwata R, Yanai K, Arai H: 2-(2-[2-dimethylaminothiazol-5-yl]ethenyl)-6-(2-[fluoro]ethoxy)benzoxazole: a novel PET agent for in vivo detection of dense amyloid plaques in Alzheimer's disease patients. *J Nucl Med* 2007;48:553–561.
- 11 Furukawa K, Okamura N, Tashiro M, Waragai M, Furumoto S, Iwata R, Yanai K, Kudo Y, Arai H: Amyloid PET in mild cognitive impairment and Alzheimer's disease with BF-227: comparison to FDG-PET. *J Neurol* 2010;257:721–727.
- 12 Verhoeff NP, Wilson AA, Takeshita S, Trop L, Hussey D, Singh K, Kung HF, Kung MP, Houle S: In vivo imaging of Alzheimer disease  $\beta$ -amyloid with [ $^{11}\text{C}$ ]SB-13 PET. *Am J Geriatr Psychiatry* 2004;12:584–595.
- 13 Okamura N, Suemoto T, Shimadzu H, Suzuki M, Shiomitsu T, Akatsu H, Yamamoto T, Staufenbiel M, Yanai K, Arai H, Sasaki H, Kudo Y, Sawada T: Styrylbenzoxazole derivatives for in vivo imaging of amyloid plaques in the brain. *J Neurosci* 2004;24:2535–2541.
- 14 Okamura N, Furumoto S, Funaki Y, Suemoto T, Kato M, Ishikawa Y, Ito S, Akatsu H, Yamamoto T, Sawada T, Arai H, Kudo Y, Yanai K: Binding and safety profile of novel benzoxazole derivative for in vivo imaging of amyloid deposits in Alzheimer's disease. *Geriatr Gerontol Int* 2007;7:393–400.
- 15 Waragai M, Okamura N, Furukawa K, Tashiro M, Furumoto S, Funaki Y, Kato M, Iwata R, Yanai K, Kudo Y, Arai H: Comparison study of amyloid PET and voxel-based morphometry analysis in mild cognitive impairment and Alzheimer's disease. *J Neurol Sci* 2009;285:100–108.
- 16 McKhann G, Drachman D, Folstein M, Katzman R, Price D, Stadlan EM: Clinical diagnosis of Alzheimer's disease: report of the NINCDS-ADRDA Work Group under the auspices of Department of Health and Human Services Task Force on Alzheimer's Disease. *Neurology* 1984;34:939–944.
- 17 Friston KJ, Holmes AP, Worsley KJ, Poline JP, Frith CD, Frackowiack RSJ: Statistical parametric maps in functional imaging: a general linear approach. *Hum Brain Mapp* 1995;2:189–210.
- 18 Matsuda H, Mizumura S, Nagao T, Ota T, Iizuka T, Nemoto K, Takemura N, Arai H, Homma A: Automated discrimination between very early Alzheimer disease and controls using an easy Z-score imaging system for multicenter brain perfusion single-photon emission tomography. *AJNR Am J Neuroradiol* 2007;28:731–736.
- 19 Okello A, Koivunen J, Edison P, Archer HA, Turkheimer FE, Någren K, Bullock R, Walker Z, Kennedy A, Fox NC, Rossor MN, Rinne JO, Brooks DJ: Conversion of amyloid positive and negative MCI to AD over 3 years: an  $^{11}\text{C}$ -PiB PET study. *Neurology* 2009;73:754–760.
- 20 Arnold SE, Hyman BT, Flory J, Damasio AR, van Hoesen GW: The topographical and neuroanatomical distribution of neurofibrillary tangles and neuritic plaques in the cerebral cortex of patients with Alzheimer's disease. *Cereb Cortex* 1991;1:103–116.
- 21 Wegiel J, Bobinski M, Tarnawski M, Dziewiatkowski J, Popovitch E, Bobinski M, Lach B, Reisberg B, Miller D, de Santi S, de Leon MJ: Shift from fibrillar to nonfibrillar A $\beta$  deposits in the neocortex of subjects with Alzheimer disease. *J Alzheimers Dis* 2001;3:49–57.
- 22 Braak H, Braak E: Neuropathological staging of Alzheimer-related changes. *Acta Neuropathol* 1991;82:239–259.
- 23 Dickson DW: The pathogenesis of senile plaques. *J Neuropathol Exp Neurol* 1997;56:321–339.
- 24 Yamaguchi H, Nakazato Y, Shoji M, Takatama M, Hirai S: Ultrastructure of diffuse plaques in senile dementia of the Alzheimer type: comparison with primitive plaques. *Acta Neuropathol* 1991;82:13–20.
- 25 Cupidi C, Capobianco R, Goffredo D, Marcon G, Ghetti B, Bugiani O, Tagliavini F, Giaccone G: Neocortical variation of A $\beta$  load in fully expressed, pure Alzheimer's disease. *J Alzheimers Dis* 2010;19:57–68.
- 26 Nelson PT, Abner EL, Scheff SW, Schmitt FA, Kryscio RJ, Jicha GA, Smith CD, Patel E, Markesbery WR: Alzheimer's-type neuropathology in the precuneus is not increased relative to other areas of neocortex across a range of cognitive impairment. *Neurosci Lett* 2009;450:336–339.



## In vivo detection of prion amyloid plaques using [ $^{11}\text{C}$ ]BF-227 PET

Nobuyuki Okamura · Yusei Shiga · Shozo Furumoto · Manabu Tashiro · Yoshio Tsuboi · Katsutoshi Furukawa · Kazuhiko Yanai · Ren Iwata · Hiroyuki Arai · Yukitsuka Kudo · Yasuhito Itoyama · Katsumi Doh-ura

Received: 7 August 2009 / Accepted: 21 October 2009 / Published online: 17 December 2009  
© Springer-Verlag 2009

### Abstract

**Purpose** In vivo detection of pathological prion protein (PrP) in the brain is potentially useful for the diagnosis of transmissible spongiform encephalopathies (TSEs). However, there are no non-invasive ante-mortem means for detection of pathological PrP deposition in the brain. The purpose of this study is to evaluate the amyloid imaging tracer BF-227 with positron emission tomography (PET) for the non-invasive detection of PrP amyloid in the brain. **Methods** The binding ability of BF-227 to PrP amyloid was investigated using autoradiography and fluorescence microscopy. Five patients with TSEs, including three patients with Gerstmann-Sträussler-Scheinker disease (GSS) and two patients with sporadic Creutzfeldt-Jakob disease (CJD), underwent [ $^{11}\text{C}$ ]BF-227 PET scans. Results were compared with data from 10 normal controls and 17 patients with Alzheimer's disease (AD). The regional to pons standard-

ized uptake value ratio was calculated as an index of BF-227 retention.

**Results** Binding of BF-227 to PrP plaques was confirmed using brain samples from autopsy-confirmed GSS cases. In clinical PET study, significantly higher retention of BF-227 was detected in the cerebellum, thalamus and lateral temporal cortex of GSS patients compared to that in the corresponding tissues of normal controls. GSS patients also showed higher retention of BF-227 in the cerebellum, thalamus and medial temporal cortex compared to AD patients. In contrast, the two CJD patients showed no obvious retention of BF-227 in the brain.

**Conclusion** Although [ $^{11}\text{C}$ ]BF-227 is a non-specific imaging marker of cerebral amyloidosis, it is useful for in vivo detection of PrP plaques in the human brain in GSS, based on the regional distribution of the tracer. PET amyloid imaging might provide a means for both early diagnosis and non-invasive disease monitoring of certain forms of TSEs.

N. Okamura · S. Furumoto · K. Yanai  
Department of Pharmacology,  
Tohoku University School of Medicine,  
Sendai, Japan

Y. Shiga · Y. Itoyama  
Department of Neurology,  
Tohoku University School of Medicine,  
Sendai, Japan

S. Furumoto · R. Iwata  
Division of Radiopharmaceutical Chemistry,  
Cyclotron and Radioisotope Center, Tohoku University,  
Sendai, Japan

M. Tashiro  
Division of Cyclotron Nuclear Medicine,  
Cyclotron and Radioisotope Center, Tohoku University,  
Sendai, Japan

Y. Tsuboi  
Department of Neurology,  
Fukuoka University School of Medicine,  
Fukuoka, Japan

K. Furukawa · H. Arai  
Department of Geriatrics and Gerontology,  
Division of Brain Sciences, Institute of Development,  
Aging, and Cancer, Tohoku University,  
Sendai, Japan

Y. Kudo  
Innovation of New Biomedical Engineering Center,  
Tohoku University,  
Sendai, Japan

K. Doh-ura (✉)  
Department of Prion Research,  
Tohoku University School of Medicine,  
2-1 Seiryomachi, Aoba-ku, Sendai 980-8575, Japan  
e-mail: doh-ura@mail.tains.tohoku.ac.jp

**Keywords** Prion · PET · Amyloid · Creutzfeldt-Jakob disease

## Introduction

Transmissible spongiform encephalopathies (TSEs), also known as prion diseases, are a group of fatal neurodegenerative disorders, including Creutzfeldt-Jakob disease (CJD), Gerstmann-Sträussler-Scheinker disease (GSS) and kuru [1–3]. TSEs are characterized by progressive deposition of abnormal prion protein (PrP) in the brain. CJD is the most common type of human TSE and is classified into sporadic, genetic and infectious forms according to the aetiology of illness. GSS is a familial neurodegenerative disorder associated with mutations of the PrP gene and is clinically recognized by cerebellar ataxia combined with postural abnormalities and cognitive decline [1–3]. Two major types of abnormal PrP deposition, synaptic and plaque types, have been described in the brain of people with TSEs [1]. The synaptic type of PrP deposition, which does not have tinctorial properties of amyloid in tissue sections, is most commonly observed in sporadic CJD, whereas the plaque type, which frequently forms congophilic amyloid plaques, is a hallmark of such TSEs as GSS, variant CJD (vCJD) and iatrogenic dura CJD with plaques [1, 4]. Abnormal PrP deposition in the brain is suggested to start before the occurrence of clinical symptoms [5–7]. Thus, preclinical diagnosis and, when available, early disease-specific therapeutic interventions, can be beneficial for people predisposed to or affected by TSEs.

Several positron emission tomography (PET) imaging agents have been recently developed and used for in vivo detection of brain amyloid- $\beta$  (A $\beta$ ) plaques in patients with Alzheimer's disease (AD) [8–12]. Most of these  $\beta$ -sheet binding agents show high binding affinity to PrP amyloid because PrP aggregates in TSEs form  $\beta$ -pleated sheet structures and share a common secondary structure with A $\beta$  deposits in AD brains [13–16]. Therefore, these agents would be useful for the in vivo detection of PrP amyloid in the brain. Two clinical PET studies were performed using [ $^{18}\text{F}$ ]FDDNP and/or [ $^{11}\text{C}$ ]PIB in sporadic and familial CJD patients [17, 18]. The results indicated moderate retention of FDDNP and no obvious retention of PIB in the brain [17, 18]. Therefore, agents that can sensitively detect abnormal PrP deposits should be further explored for the diagnosis of TSEs. We have demonstrated in vitro and in vivo binding of benzoxazole derivatives to both A $\beta$  and PrP amyloids [19, 20]. One of these derivatives, BF-227, was used for a clinical PET study where it successfully visualized amyloid deposits in the brain of AD patients in vivo [12, 21]. Therefore, [ $^{11}\text{C}$ ]BF-227 appears to be a promising candidate for PET imaging of PrP deposits. The

purpose of this study was to evaluate the clinical utility of [ $^{11}\text{C}$ ]BF-227 PET for the non-invasive detection of abnormal PrP deposits in patients with TSEs.

## Methods

### Preparation of compounds

BF-227 and its 2-tosyloxyethoxy and *N*-desmethylated derivatives were custom synthesized by Tanabe R&D Service Co. (Osaka, Japan). [ $^{18}\text{F}$ ]BF-227 was synthesized for autoradiography of brain sections, as described previously [22]. For the clinical studies, [ $^{11}\text{C}$ ]BF-227 was synthesized as described previously [12]. Radiochemical yields were greater than 50% based on [ $^{11}\text{C}$ ]methyl triflate, and specific radioactivities were 119–138 GBq/ $\mu\text{mol}$  at the end of synthesis. Radiochemical purities were greater than 95%.

### Histopathological staining and in vitro autoradiography

Autopsy-diagnosed brain samples from two GSS cases with PrP plaque deposition and two sporadic CJD cases with synaptic PrP deposition were provided by Dr. Toru Iwaki of the Department of Neuropathology, Kyushu University, Japan. The brain sample from an 81-year-old man with autopsy-confirmed physiological aging was obtained from Tohoku University Hospital. The two GSS cases had a proline-to-leucine mutation at codon 102 and methionine homozygosity at codon 129 of the PrP gene, and the two sporadic CJD cases had no mutations and methionine homozygosity at codon 129; they showed type 1 abnormal PrP in immunoblotting of the brain tissues. All of the brain samples were treated with 98% formic acid for 1 h before paraffin embedding to eliminate prion infectivity. Sections from paraffin-embedded blocks of the cerebellum or frontal cortex were then dewaxed in xylene and ethanol. For staining with BF-227, tissue sections were immersed in 100  $\mu\text{M}$  BF-227 solution containing 50% ethanol for 10 min. They were then dipped briefly into water and rinsed in phosphate-buffered saline for 10 min before coverslipping with FluorSave Reagent (Calbiochem, La Jolla, CA, USA). Subsequently, they were examined using an Eclipse E800 microscope (Nikon, Tokyo, Japan) equipped with a V-2A filter set (excitation, 380–420 nm; dichroic mirror, 430 nm; Longpass filter, 450 nm). For autoradiography, the section was incubated with 1.0 MBq/ml of [ $^{18}\text{F}$ ]BF-227 at room temperature for 10 min and then washed briefly with water and 50% ethanol. After drying, the labelled section was exposed to a BAS-III imaging plate (Fuji Film, Tokyo, Japan) overnight. Autoradiographic images were obtained using a BAS-5000 phosphor imaging instrument (Fuji Film, Tokyo, Japan). Neighbouring sec-

tions were immunostained using 3F4 anti-PrP monoclonal antibody (Covance, Princeton, NJ, USA) as described previously [13, 20].

#### Subjects and patients in the clinical PET study

Five TSE patients, including two sporadic CJD patients [63-year-old woman (CJD1) and 58-year-old man (CJD2)] and three GSS patients [69-year-old woman (GSS1), 61-year-old man (GSS2) and 30-year-old woman (GSS3)], underwent PET scans with [<sup>11</sup>C]JBF-227 (Table 1). For comparison, [<sup>11</sup>C]JBF-227 PET studies were also performed in 17 AD patients [mean age ± standard deviation (SD)=72.6±6.7; mean Mini-Mental State Examination score ± SD=19.8±4.0] and 10 aged normal controls (mean age ± SD=67.2±2.5). Some of these AD and normal subjects were included in our previous report [12].

CJD1's health was unremarkable until the manifestation of depressive symptoms at the age of 62 years. The patient then developed subacutely progressive dementia, motor disturbances and myoclonus. CJD2 showed subacutely progressive dementia and gait disturbance and then developed psychotic symptoms, dysarthria and myoclonus. Both CJD patients had no mutations and showed methionine homozygosity at codon 129 of the PrP gene. PET studies in CJD1 and CJD2 were performed when they reached grade 4 of the modified Rankin scale at 3 and 4 months after onset of symptoms, respectively. Both patients showed periodic synchronous discharges in electroencephalograms and hyperintensity in the caudate, putamen and cerebral cortex on diffusion-weighted magnetic resonance (MR) images. Diagnosis of probable CJD was made according to the WHO criteria [23].

Each GSS patient was from a different pedigree and had a family history of the same disease, carrying a proline-to-leucine mutation at codon 102 and methionine homozy-

gosity at codon 129 of the PrP gene. GSS1 and GSS2, having a 9- and 20-month clinical duration from the onset, respectively, showed signs of moderate cerebellar ataxia, such as gait disturbance and slurred speech; however, they could walk unassisted and had slight or no cognitive impairment. GSS1 and GSS2 scored 22 and 26 points, respectively, on the Mini-Mental State Examination. GSS3, having a 27-month clinical duration, showed severe gait disturbance and slurred speech and was unable to walk unassisted; however, she had no cognitive impairment (30 points on the Mini-Mental State Examination) at the time of this study.

AD diagnosis was made according to the National Institute of Neurological and Communicative Diseases and Stroke-Alzheimer's Disease and Related Disorders Association (NINCDS-ADRDA) criteria [24]. CJD, GSS and AD patients were recruited from Miyagi National Hospital, Fukuoka University Hospital, Kagoshima University Hospital and Tohoku University Hospital. Normal controls were recruited from volunteers with no cognitive impairment or cerebrovascular lesions on MR images and who were not taking any centrally acting medications. No significant difference in age distribution was apparent between the groups. This study was approved by the Ethics Committee on clinical investigations of Tohoku University School of Medicine and performed in accordance with the Declaration of Helsinki. Written informed consent was obtained after complete description of the study to the patients and subjects.

#### Image acquisition protocols

PET scans were performed using a SET-2400W (Shimadzu Inc., Kyoto, Japan). After intravenous injection of 211–366 MBq (5.7–9.9 mCi) of [<sup>11</sup>C]JBF-227, dynamic PET images were obtained for 60 min with the subjects' eyes closed. Arterial blood sampling in the TSE patients was not

**Table 1** Regional to pons standardized uptake value ratio (SUVr<sub>p</sub>) values in aged normal controls (Control), Alzheimer's disease patients (AD), Creutzfeldt-Jakob disease patients (CJD) and Gerstmann-Sträussler-Scheinker disease patients (GSS)

	Control (n=10) Mean ± SD	AD (n=17) Mean ± SD	CJD1	CJD2	GSS (n=3) Mean ± SD	GSS1	GSS2	GSS3
Frontal	0.60±0.03	0.64±0.04	0.57	0.61	0.67±0.08	0.74	0.69	0.57
Lateral temporal	0.59±0.03	0.69±0.04*	0.63	0.62	0.67±0.05*	0.71	0.68	0.61
Parietal	0.62±0.02	0.69±0.04*	0.62	0.62	0.67±0.06	0.72	0.68	0.61
Occipital	0.62±0.04	0.65±0.05	0.62	0.69	0.67±0.07	0.74	0.67	0.60
Medial temporal	0.64±0.04	0.62±0.03	0.57	0.65	0.67±0.02**	0.66	0.70	0.67
Striatum	0.71±0.04	0.75±0.04*	0.69	0.72	0.76±0.04	0.80	0.77	0.72
Thalamus	1.00±0.04	1.01±0.04	0.97	1.04	1.08±0.00*, **	1.08	1.07	1.08
Cerebellum	0.58±0.01	0.57±0.02	0.58	0.59	0.62±0.01*, **	0.61	0.63	0.61

\**p*<0.05 compared to aged normal group

\*\**p*<0.05 compared to AD group

performed because the Committee on Clinical Investigation at Tohoku University School of Medicine did not approve blood sampling during the PET scan, from the standpoint of infection risk management. T<sub>1</sub>-weighted MR images were obtained using a Signa 1.5-T machine (General Electric Inc., Milwaukee, WI, USA).

#### Image analysis

Standardized uptake value (SUV) images of [<sup>11</sup>C]BF-227 were obtained by normalizing tissue concentration by injected dose and body weight. Average summations of SUV images were created from early frames (0–30 min post-injection) and late frames (40–60 min post-injection) of dynamic PET images. Early frame images were created for co-registration with individual MR images, and late frame images were used for calculation of SUV. Individual MR images were anatomically co-registered with the early frame PET images using statistical parametric mapping software (SPM2, Wellcome Department of Imaging Neuroscience, London, UK) [25]. Spatial normalization was performed using an MR T<sub>1</sub> template of SPM2 to transfer PET images into a standard stereotactic space. Regions of interest (ROIs) were placed on a spatially normalized MR image, as described previously [12]. ROI information was then copied onto delayed PET SUV images, and regional SUV images at 40–60 min post-injection were sampled using Dr.View/LINUX software (AJS, Tokyo, Japan). Deposition of PrP plaques is reportedly frequent in the cerebellum but scarce in the pons of GSS brain [26].

Furthermore, BF-227 retention in the pons does not differ between AD patients and normal controls. Therefore, we used the pons as a reference region and calculated the regional to pons SUV ratio (SUVRp) as an index of BF-227 retention.

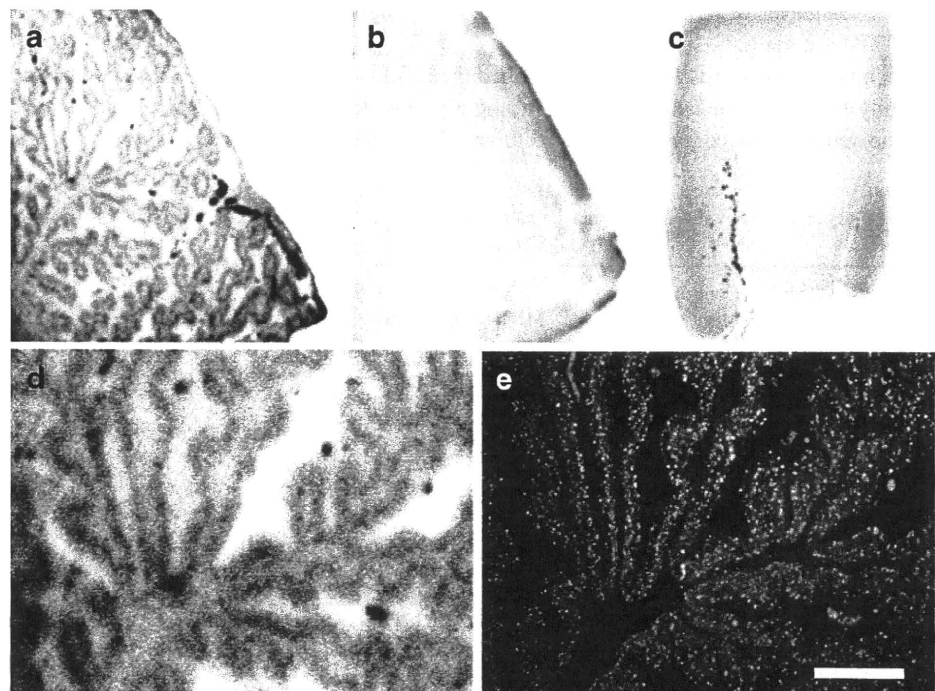
#### Statistical analysis

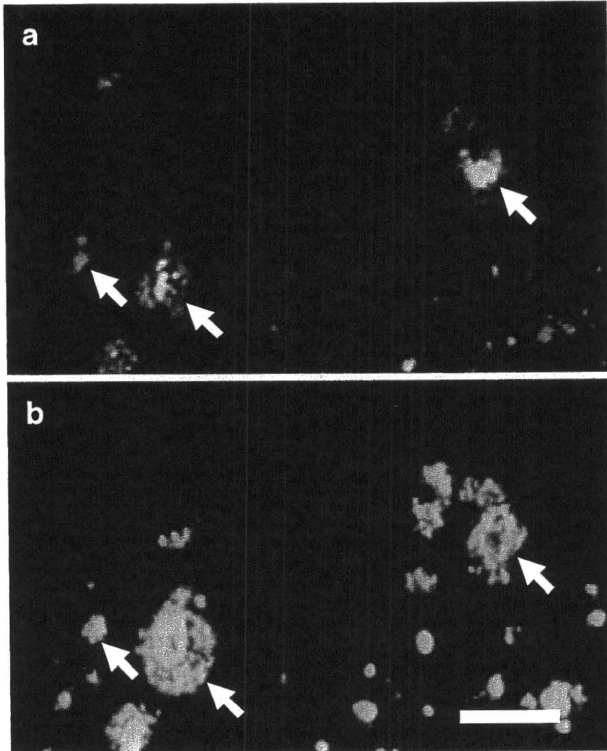
For statistical comparison in each group, we applied one-way analysis of variance, followed by the Bonferroni-Dunn post hoc test. Statistical comparison of age distribution was performed using the Kruskal-Wallis test, followed by Dunn's multiple comparison test. Statistical significance for each analysis was defined as  $p < 0.05$ .

#### Results

Autoradiography examination indicated binding of a tracer dose of BF-227 to PrP plaque deposits. BF-227 retention was present in brain sections from GSS cases with PrP plaque deposition but not from normal control cases and sporadic CJD cases with synaptic PrP deposition (Fig. 1a–c). The regional distribution of [<sup>18</sup>F]BF-227 in the autoradiograms co-localized with the immunostained PrP plaques in the cerebellar cortex of GSS cases (Fig. 1d–e). BF-227 binding to PrP plaques was additionally examined using a microscope, because BF-227 is a fluorescent compound. Core regions of the PrP plaques were intensely stained with BF-227 (Fig. 2, arrows), indicating that BF-227 preferentially binds to the fibril-rich core of PrP amyloid plaques.

**Fig. 1** [<sup>18</sup>F]BF-227 autoradiograms of a cerebellar section from a Gerstmann-Sträussler-Scheinker (GSS) case (a), a cerebellar section from a physiological aging case (b) and a frontal cortex section from a sporadic Creutzfeldt-Jakob disease (CJD) case (c) are shown, together with a magnified view of a (d) and prion protein (PrP) immunostaining of the same field as d (e). BF-227 retention was present in the brain section from a GSS case with PrP plaque deposition, but not from a normal control case and sporadic CJD case with synaptic PrP deposition. Bar=200 μm





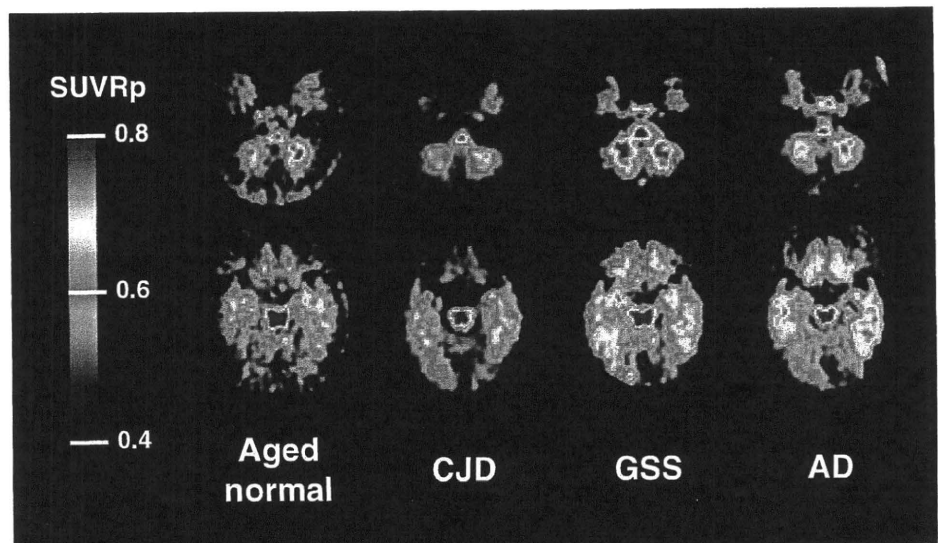
**Fig. 2** Microscopic images of BF-227 staining (a) and PrP immunostaining (b) of the cerebellar cortex of a GSS case. Arrows indicate PrP amyloid plaques. The core regions of PrP plaques were intensely stained with BF-227. Bar=50  $\mu$ m

Figure 3 shows the average summations of SUVRp images in an aged normal subject (64-year-old man), a sporadic CJD patient (CJD1, 63-year-old woman), a GSS patient (GSS2, 61-year-old man) and an AD patient (62-year-old woman). As reported previously, non-specific retention of [ $^{11}$ C]BF-227 was observed in the brain stem

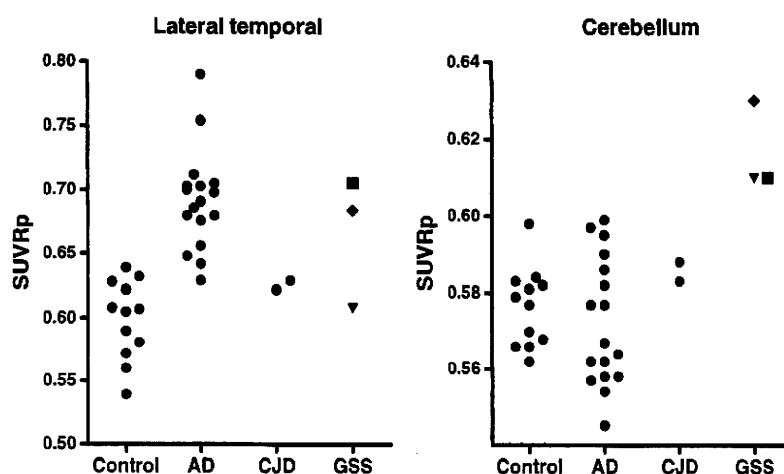
and white matter of all subjects [12]. The GSS patient showed obvious retention of [ $^{11}$ C]BF-227 in the cerebellum, and lateral and medial temporal cortices. The three GSS patients showed significantly higher SUVRp in the lateral temporal cortex, thalamus and cerebellum (Table 1, Fig. 4) when compared to aged normal controls. Furthermore, when compared to the AD group, the GSS group showed significant elevation of SUVRp in the medial temporal cortex, thalamus and cerebellum. Although two GSS patients (GSS1 and GSS2) showed retention of BF-227 in most brain regions, the youngest GSS patient (GSS3) showed BF-227 retention only in the cerebellum, thalamus and medial temporal cortex, but not in the neocortex (Table 1, Fig. 4). Furthermore, two sporadic CJD patients showed no obvious BF-227 retention in any of the brain regions examined (Table 1, Fig. 4). As previously described [12, 21], AD patients showed [ $^{11}$ C]BF-227 retention in the neocortex; however, the cerebellum and medial temporal cortex were relatively spared (Table 1).

Autopsy examination of the brain of one GSS patient (GSS1) confirmed both the presence of abundant PrP amyloid plaques in the neocortex, cerebellum, basal ganglia, thalamus, entorhinal cortex and hippocampus and the absence of A $\beta$  amyloid plaques or other structures of misfolded protein deposition such as Lewy bodies and neurofibrillary tangles. When compared to controls, the highest SUVRp percentage difference was found in the neocortex, especially in the frontal cortex (22%), followed by the striatum (12%), thalamus (9%), cerebellum (6%) and medial temporal cortex (3%) in this case. This finding was consistent with the autopsy result showing higher density of PrP amyloid plaques in the neocortex and basal ganglia than in the cerebellum, thalamus and hippocampus. Details of clinicopathological features of this case will be published elsewhere.

**Fig. 3** Mean regional to pons standardized uptake value ratio (SUVRp) images between 40 and 60 min post-injection of [ $^{11}$ C]BF-227 in an aged normal subject (64-year-old man), a sporadic CJD patient (CJD1, 63-year-old woman), a GSS patient (GSS2, 61-year-old man) and an AD patient (62-year-old woman). Compared to the aged normal subject and CJD patient, the GSS patient showed obvious [ $^{11}$ C]BF-227 retention in the cerebellum and temporal cortex. The AD patient also showed obvious [ $^{11}$ C]BF-227 retention in the temporal cortex; however, the cerebellum was relatively spared



**Fig. 4** SUVRp distribution in aged normal controls (*Control*), AD patients (*AD*), CJD patients (*CJD*) and GSS patients (*GSS*). GSS patients showed higher SUVRp values in the lateral temporal cortex and cerebellum. Filled square GSS1, filled diamond GSS2, filled inverted triangle GSS3



## Discussion

This is the first study to demonstrate non-invasive detection of PrP amyloid plaques in GSS patients. GSS is neuropathologically characterized by deposits of multicentric amyloid plaques, which are especially abundant in the cerebellum, cerebral cortex and basal ganglia [3]. The present study demonstrated binding of BF-227 to PrP amyloid plaques in GSS brain sections. [ $^{11}\text{C}$ ]BF-227 retention was observed in cortical and subcortical brain regions of GSS patients known for the high density of PrP plaques. Based on these findings, [ $^{11}\text{C}$ ]BF-227 represents a promising candidate PET probe for the non-invasive detection of PrP amyloid plaques in the brain. However, the possibility that neocortical elevation of SUVRp in GSS patients might be caused by concomitant A $\beta$  amyloid deposits or other misfolded protein deposits also should be considered, given that the two GSS patients showing prominent neocortical retention of [ $^{11}\text{C}$ ]BF-227 were relatively older than the GSS patient showing no neocortical retention of BF-227. Although one positive GSS patient (GSS2) is still alive and was not examined neuropathologically, another positive case (GSS1) showed a high level of PrP amyloid deposits but no obvious deposits of A $\beta$  amyloid or other misfolded proteins at autopsy. Furthermore, significant elevation of SUVRp was detected in the cerebellum, thalamus and hippocampus of all GSS cases. These brain regions are known to contain lower densities of A $\beta$  plaques or other misfolded protein structures such as Lewy bodies. Based on these findings, it seems unlikely that concomitant deposition of A $\beta$  amyloid or other misfolded proteins contributes to the high [ $^{11}\text{C}$ ]BF-227 retention in GSS patients.

There is an increasing demand for *in vivo* detection of abnormal PrP deposition in the brain for the diagnosis of TSEs that might translate in early therapeutic intervention. Although GSS and other familial forms of TSEs can be diagnosed with

PrP gene analysis using peripheral blood cells, it has been impossible to non-invasively measure the amount of abnormal PrP deposition in the brain. In a fashion similar to GSS, PrP amyloid deposition in the brain is commonly present in vCJD in which PrP amyloid plaques, called florid plaques, are pathognomonic [27]. Thus, [ $^{11}\text{C}$ ]BF-227 PET might be a sensitive probe for the detection of PrP amyloid plaque deposition in vCJD as well as GSS, allowing longitudinal monitoring of PrP amyloid plaque deposition in the brain. Ante-mortem diagnosis of vCJD relies on the detection of abnormal PrP deposition in tonsil biopsy samples [28]. However, functional imaging using PET has an advantage over surgical biopsy tests in terms of both a non-invasive and an infection risk management point of view.

GSS is a rare form of TSE occurring in only about 3% of TSE cases in Japan. However, GSS is probably one of the TSEs most likely to benefit from early therapeutic interventions because the disease can be confirmed earlier using PrP gene analysis and progression occurs much more slowly than that in sporadic CJD, which comprises the majority of TSE cases. Recently, compounds such as pentosan polysulphate and doxycycline have been clinically used for experimental treatments for TSEs to prevent deposition of abnormal PrP in the brain, because these compounds slowed the disease progression in animal disease models when administered in an earlier stage of the disease [29–33]. Reliable surrogate markers are also required to evaluate the efficacy of these experimental interventions, and [ $^{11}\text{C}$ ]BF-227 PET might be one of the best candidates to assess PrP amyloid deposition in GSS. However, it remains to be elucidated if PrP amyloid levels are a particularly relevant marker of therapeutic efficacy.

A previous PET study demonstrated moderate FDDNP retention and no remarkable PIB retention in the brain of two familial CJD patients with an octapeptide repeat insertion mutation [17]. A recent PET study has additionally demonstrated no PIB retention in two autopsy-confirmed sporadic

CJD patients [18]. In contrast with these studies, the present study successfully demonstrated prominent [ $^{11}\text{C}$ ]BF-227 retention in the brain of GSS patients. Differences between the previous and present findings might mainly reside in the amount and type of PrP amyloid deposits in the brain, where histopathological studies indicate higher density of PrP amyloid plaques in GSS than in familial CJD [1]. In the present study, the findings in two sporadic CJD patients showing no obvious [ $^{11}\text{C}$ ]BF-227 retention in the brain additionally support this speculation. The difference may also be attributable to higher binding affinity of BF-227 to PrP amyloid cores compared to FDDNP and PIB. To clarify this, further in vitro studies comparing the binding affinities of different amyloid tracers to PrP plaques in TSE brain homogenates are needed.

The youngest GSS patient (GSS3) showed BF-227 retention in the cerebellum and thalamus but not in the neocortex. The clinical symptoms in this patient were consistent with the brain distribution of BF-227, with the patient presenting with severe gait disturbance and slurred speech resulting from cerebellar ataxia but no signs of cognitive impairment, suggesting a close relationship between PrP plaque deposition as measured by BF-227 and regional brain dysfunction. There are variations of clinical phenotypes in GSS [1, 3]. Such variations are yet to be explained; however, the pattern of regional PrP amyloid distribution might be one of the factors affecting clinical phenotypes of GSS. In vivo PrP amyloid imaging using [ $^{11}\text{C}$ ]BF-227 or other PET tracers will clarify neuropathological aspects of clinical variations in GSS.

In summary, we confirmed binding of BF-227 to PrP plaques in vitro and in vivo. A clinical PET study using [ $^{11}\text{C}$ ]BF-227 demonstrated in vivo detection of PrP amyloid plaques in GSS patients. This imaging technique provides a potential means of facilitating both early diagnosis and non-invasive disease monitoring of certain forms of TSEs because, despite a lack of selectivity for PrP, brain retention of BF-227 in GSS shows a distinct pattern of regional distribution than that usually observed in sporadic AD.

**Acknowledgment** We appreciate the assistance of Dr. S. Watanuki, Dr. M. Miyake and Dr. H. Takashima in the clinical PET studies. This study was supported in part by the Program for the Promotion of Fundamental Studies in Health Science of the NIBIO in Japan, Industrial Technology Research Grant Program of the NEDO in Japan, and Health and Labor Sciences Research Grants (Translational Research and Research on Measures for Intractable Diseases) from the Ministry of Health, Labor, and Welfare of Japan.

## References

- DeArmond SJ, Kretschmar HA, Prusiner SB. Prion diseases. In: Graham DI, Lantos PL, editors. *Greenfield's neuropathology*, 7th ed. London: Hodder Arnold. p. 273–323.
- Collins SJ, Lawson VA, Masters CL. Transmissible spongiform encephalopathies. *Lancet* 2004;363:51–61.
- Collins S, McLean CA, Masters CL. Gerstmann-Sträussler-Scheinker syndrome, fatal familial insomnia, and kuru: a review of these less common human transmissible spongiform encephalopathies. *J Clin Neurosci* 2001;8:387–97.
- Noguchi-Shinohara M, Hamaguchi T, Kitamoto T, Sato T, Nakamura Y, Mizusawa H, et al. Clinical features and diagnosis of dura mater graft associated Creutzfeldt-Jakob disease. *Neurology* 2007;69:360–7.
- Lasmézas CI, Deslys JP, Demaimay R, Adjou KT, Hauw JJ, Dormont D. Strain specific and common pathogenic events in murine models of scrapie and bovine spongiform encephalopathy. *J Gen Virol* 1996;77(Pt 7):1601–9.
- Schulz-Schaeffer WJ, Tschöke S, Kranefuss N, Dröse W, Hause-Reitner D, Giese A, et al. The paraffin-embedded tissue blot detects PrP(Sc) early in the incubation time in prion diseases. *Am J Pathol* 2000;156:51–6.
- Fraser JR. What is the basis of transmissible spongiform encephalopathy induced neurodegeneration and can it be repaired? *Neuropathol Appl Neurobiol* 2002;28:1–11.
- Small GW, Kepe V, Ercoli LM, Siddarth P, Bookheimer SY, Miller KJ, et al. PET of brain amyloid and tau in mild cognitive impairment. *N Engl J Med* 2006;355:2652–63.
- Klunk WE, Engler H, Nordberg A, Wang Y, Blomqvist G, Holt DP, et al. Imaging brain amyloid in Alzheimer's disease with Pittsburgh Compound-B. *Ann Neurol* 2004;55:306–19.
- Verhoeff NP, Wilson AA, Takeshita S, Trop L, Hussey D, Singh K, et al. In-vivo imaging of Alzheimer disease beta-amyloid with [ $^{11}\text{C}$ ]SB-13 PET. *Am J Geriatr Psychiatry* 2004;12:584–95.
- Rowe CC, Ackerman U, Browne W, Mulligan R, Pike KL, O'Keefe G, et al. Imaging of amyloid beta in Alzheimer's disease with 18F-BAY94-9172, a novel PET tracer: proof of mechanism. *Lancet Neurol* 2008;7:129–35.
- Kudo Y, Okamura N, Furumoto S, Tashiro M, Furukawa K, Maruyama M, et al. 2-(2-[2-Dimethylaminothiazol-5-yl]ethenyl)-6-(2-[fluoro]ethoxy)benzoxazole: a novel PET agent for in vivo detection of dense amyloid plaques in Alzheimer's disease patients. *J Nucl Med* 2007;48:553–61.
- Ishikawa K, Doh-ura K, Kudo Y, Nishida N, Murakami-Kubo I, Ando Y, et al. Amyloid imaging probes are useful for detection of prion plaques and treatment of transmissible spongiform encephalopathies. *J Gen Virol* 2004;85:1785–90.
- Bresjanac M, Smid LM, Vovko TD, Petric A, Barrio JR, Popovic M. Molecular-imaging probe 2-(1-[6-[(2-fluoroethyl)(methyl)amino]-2-naphthyl]ethylidene) malononitrile labels prion plaques in vitro. *J Neurosci* 2003;23:8029–33.
- Sadowski M, Pankiewicz J, Scholtzova H, Tsai J, Li Y, Carp RI, et al. Targeting prion amyloid deposits in vivo. *J Neuropathol Exp Neurol* 2004;63:775–84.
- Hoefert VB, Aiken JM, McKenzie D, Johnson CJ. Labeling of the scrapie-associated prion protein in vitro and in vivo. *Neurosci Lett* 2004;371:176–80.
- Boxer AL, Rabinovici GD, Kepe V, Goldman J, Furst AJ, Huang SC, et al. Amyloid imaging in distinguishing atypical prion disease from Alzheimer disease. *Neurology* 2007;69:283–90.
- Villemagne VL, McLean CA, Reardon K, Boyd A, Lewis V, Klug G, et al. 11C-PIB PET studies in typical sporadic Creutzfeldt-Jakob disease. *J Neurol Neurosurg Psychiatry* 2009;80:998–1001. doi:10.1136/jnnp.2008.171496.
- Okamura N, Suemoto T, Shimadzu H, Suzuki M, Shiomitsu T, Akatsu H, et al. Styrylbenzoxazole derivatives for in vivo imaging of amyloid plaques in the brain. *J Neurosci* 2004;24:2535–41.
- Ishikawa K, Kudo Y, Nishida N, Suemoto T, Sawada T, Iwaki T, et al. Styrylbenzoxazole derivatives for imaging of prion plaques and treatment of transmissible spongiform encephalopathies. *J Neurochem* 2006;99:198–205.

21. Waragai M, Okamura N, Furukawa K, Tashiro M, Furumoto S, Funaki Y, et al. Comparison study of amyloid PET and voxel-based morphometry analysis in mild cognitive impairment and Alzheimer's disease. *J Neurol Sci* 2009;285:100–8. doi:10.1016/j.jns.2009.06.005.
22. Okamura N, Furumoto S, Funaki Y, Suemoto T, Kato M, Ishikawa Y, et al. Binding and safety profile of novel benzoxazole derivative for in vivo imaging of amyloid deposits in Alzheimer's disease. *Geriatr Gerontol Int* 2007;7:393–400.
23. Zeidler M, Gibbs CJ Jr, Meslin F. WHO manual for strengthening diagnosis and surveillance of Creutzfeldt-Jakob disease. Geneva: World Health Organization; 1998. p. 47–51.
24. McKhann G, Drachman D, Folstein M, Katzman R, Price D, Stadlan EM. Clinical diagnosis of Alzheimer's disease: report of the NINCDS-ADRDA Work Group under the auspices of Department of Health and Human Services Task Force on Alzheimer's Disease. *Neurology* 1984;34:939–44.
25. Friston KJ, Holmes AP, Worsley KJ, Poline JP, Frith CD, Frackowiack RSJ. Statistical parametric maps in functional imaging: a general linear approach. *Hum Brain Mapp* 1995;2:189–210.
26. Masters CL, Gajdusek DC, Gibbs CJ Jr. Creutzfeldt-Jakob disease virus isolations from the Gerstmann-Sträussler syndrome with an analysis of the various forms of amyloid plaque deposition in the virus-induced spongiform encephalopathies. *Brain* 1981;104:559–88.
27. Ironside JW, McCardle L, Horsburgh A, Lim Z, Head MW. Pathological diagnosis of variant Creutzfeldt-Jakob disease. *APMIS* 2002;110:79–87.
28. Hill AF, Zeidler M, Ironside J, Collinge J. Diagnosis of new variant Creutzfeldt-Jakob disease by tonsil biopsy. *Lancet* 1997;349:99–100.
29. Doh-ura K, Ishikawa K, Murakami-Kubo I, Sasaki K, Mohri S, Race R, et al. Treatment of transmissible spongiform encephalopathy by intraventricular drug infusion in animal models. *J Virol* 2004;78:4999–5006.
30. Rainov NG, Tsuboi Y, Krolak-Salmon P, Vighetto A, Doh-Ura K. Experimental treatments for human transmissible spongiform encephalopathies: is there a role for pentosan polysulfate? *Expert Opin Biol Ther* 2007;7:713–26.
31. De Luigi A, Colombo L, Diomedea L, Capobianco R, Mangieri M, Miccolo C, et al. The efficacy of tetracyclines in peripheral and intracerebral prion infection. *PLoS One* 2008;3:e1888.
32. Teruya K, Kawagoe K, Kimura T, Chen CJ, Sakasegawa Y, Doh-ura K. Amyloidophilic compounds for prion diseases. *Infect Disord Drug Targets* 2009;9:15–22.
33. Forloni G, Salmona M, Marcon G, Tagliavini F. Tetracyclines and prion infectivity. *Infect Disord Drug Targets* 2009;9:23–30.



## MCI の概念と preclinical AD の提唱

## Mild cognitive impairment and proposal of preclinical Alzheimer's disease

東北大学加齢医学研究所脳科学研究部門老年医学分野教授

Hiroyuki Arai 荒井啓行

東北大学病院老年科准教授

Katsutoshi Furukawa 古川勝敏

東北大学未来医工学治療開発センター教授

Yukitsuka Kudo 工藤幸司

東北大学病院老年科

Naoki Tomita 富田尚希

## Summary

Mild cognitive impairment (MCI) とは、正常でもない、認知症でもないグレイゾーンを指す。この MCI は臨床的にも病因論的にも多様であるが、その定義上、認知症に近い late MCI と正常に近い early MCI の 2 アームがある。Early MCI よりさらに正常に近い状態でありながら PET 画像や脳脊髄液バイオマーカーなどの客観的指標が正常を逸脱しアルツハイマー病 (AD) パターンを示しはじめた段階を preclinical AD と呼ぶことが 2010 年 7 月米国アルツハイマー病協会から提唱された。Preclinical AD 段階からの根本治療に注目が向けられている。

## Key words

- 軽度認知障害 (MCI)
- 予防戦略 (prevention strategy)
- Clinical Trials of Alzheimer's Disease (CTAD)
- preclinical AD
- アミロイド仮説
- 根本治療薬

## I MCI の概念

1995年の東京都における調査では、80歳台では約20%、90歳台では約40%、100歳以上に至っては90%以上の高齢者が程度の差こそあれ、認知症を患っているという事実が明らかにされた。「人類は長生きの代償として認知症と向き合わなければならないのか」こんな現実が浮き彫りにされたのである。日本では古くから70歳=古希、80歳=傘寿、90歳=卒寿と呼んで長寿を祝ってきたが、認知症になってしまうと、心からお祝いをするという気持ちにもなれないであろう。認知症では外見は同じでも脳が変貌していく姿は恐ろしくすらある。一般に、認知症とは「一度獲得された知的機能の後天的な障害によって、日常生活機能を喪失した状態」と考えられている。この定義から明らかなように、ごく普通の自立生活を営んでいた高齢者がいつとはなしに正常を逸脱し認知症患者となっていくのである(図1)。別のいい方をすれば、認知症患者も少し前までは全くの正常高齢者であったわけである。しかもその可能性は誰にでもある。正常から認知症へと変貌する過程で、正常でもないが認知症ともいえない段階が存在する。これが軽度認知障害(mild cognitive impairment; MCI)である<sup>1)</sup>。より直截的に MCI を定義するとすれば、MCI とは「正常でもないし、

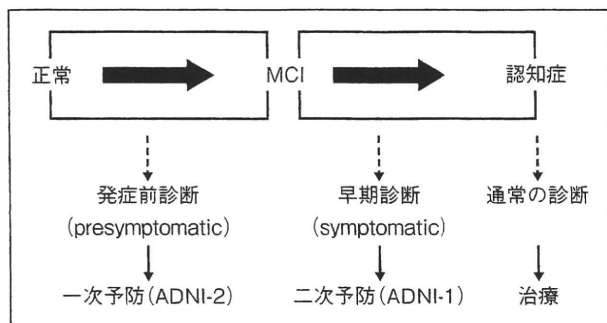


図1 正常から認知症への連続スペクトラム  
 正常を逸脱し認知症に至る過程は約20年を要する連続的移行といえる。正常でもない、かつ認知症でもない中間的段階は mild cognitive impairment (MCI) と呼ばれているが、認知症により近い段階が late MCI、正常により近い段階が early MCI とされている。Late MCI の段階では、病理像はおおむね完成しており神経細胞の著しい脱落がみられる。今後米国で立ち上げられる ADNI-2 では、正常から early MCI への過程が焦点となると考えられる。

認知症でもない中間的「グレーゾーン」となるであろう。より操作的に考えれば、①記憶障害は明らかであるが、その他の認知機能はおおむね正常で日常生活に大きな影響が及んでいない場合、あるいは②軽度の記憶力低下、言語機能低下、視空間機能低下、注意分割機能低下など複数の高次機能障害があるが、その総和としての機能低下が認知症といえるレベルにまで達していない場合は、MCI と呼ぶことが適当と思われる。MCI は臨床的にも病因論的にも多様であるが<sup>2)</sup>、その定義上、認知症ステージに近い late MCI と正常に近い early MCI の異なる2つのアームがある。認知症すなわち「一度獲得された知的機能の後天的な障害によって、日常生活機能を喪失した状態」に至ってからコリンエステラーゼ阻害薬などによる保険薬治療が開始されるのが現状であるが、図1に示すように、もしこの late MCI から認知症に進行する過程がブロックされれば二次予防(secondary prevention)、また正常から early MCI への進行が阻止できれば一次予防(primary prevention)と認知症医療に大きな発展が期待されている。そのための予防戦略(prevention strategy)を構築するのも今後の ADNI (Alzheimer's Disease Neuroimaging Initiative) の大きな仕事である<sup>3)</sup>。

## II Late MCI と early MCI

ADNI に関しての総説は最近の文献を参照いただきたい<sup>3)-6)</sup>。2010年9月24日現在、J-ADNI (主任研究者：東京大学 岩坪威氏) では、149名の正常者、192名の健忘型 MCI 患者、80名の初期アルツハイマー病 (Alzheimer's disease; AD) 患者の計421名の登録を完了した。スクリーニングで組み入れ不可となったケースは103例に上った。健忘型 MCI 患者の基準としては、本人からの記憶障害の訴えに加えて介護者の立場の者がそれを容認する、あるいは本人からの記憶障害の訴えはなくても、介護者から記憶障害の事実が示されることのいずれかであることに加えて、認知機能検査では、

- ① Mini-Mental State Examination (MMSE) は24~30点である
  - ② 教育年数を考慮したウェクスラー記憶検査改訂版における論理記憶の遅延再生課題 (25点満点でスコアのよいほど記憶力は維持されている) における点数がカットオフ値以下である  
 [カットオフ値]  
 教育年数0~9年：2点あるいはそれ以下  
 教育年数10~15年：4点あるいはそれ以下  
 教育年数16年以上：8点あるいはそれ以下
  - ③ Clinical Dementia Rating (CDR) は0.5である
  - ④ うつ病ではないこと
- を満たすものを健忘型 MCI としてエントリーすることになっている。この基準に従うと①③④を満たしてもたとえば教育年数12年 (高等学校卒業レベル) の学歴の人が②のウェクスラー記憶検査改訂版で8点であった場合は、健忘型 MCI には組み入れられないことになる。高等学校卒業レベルの学歴の人は25項目のウェクスラー記憶検査改訂版で最大4項目の遅延再生しかできないほど進行してはじめて健忘型 MCI と判定される。脱落例が103例に上った理由の1つはここにある。したがって、AD に近づいてきた後半の MCI (late MCI) をエントリーし、AD への移行状況を観察するのが現在走っている ADNI といえよう。しかし、このレベルに至るまでには

正常に近い、より早期の MCI 段階があったことは容易に想像される。2009年10月から米国で開始されている ADNI-GO (grand opportunity) プロジェクトでは ADNI-1 では対象とならなかった early MCI をエントリーし2年間の観察研究を行っている。Early MCI と late MCI を比較すると、CDR、MMSE のカットオフ値は同じであるが、ウェクスラー記憶検査改訂版における論理記憶の遅延再生課題の範囲が、たとえば教育年数12年であれば5~9点であるため、上述した症例(8点)は組み入れ可能となる。また ADNI-1 ではアミロイド PET のプローブとして<sup>11</sup>C-PIB (Pittsburgh compound B) が採用されていたが、ADNI-GO では<sup>18</sup>F で標識された AV-45 プローブを用いたアミロイド PET を全例に施行予定である。<sup>11</sup>C 標識体は半減期が短く、原則サイクロトロンのある施設でなければ利用不可能であるのに対し、<sup>18</sup>F 標識体は半減期が長くラジオアイソトープ配給元からの供給を受ければ、施設内にサイクロトロンがなくても利用が可能のため、今後は<sup>18</sup>F-AV-45 を中心とした<sup>18</sup>F 標識体が汎用されていくであろう。ADNI-GO の後には ADNI-2 が計画されている<sup>3)</sup>。ADNI-2 では正常、early MCI、late MCI、初期 AD の4つの集団をエントリー対象とし、主として正常から early MCI への移行状況を観察することが大きな目玉となるであろう。ADNI-2 の期間は5年間で、ADNI-1 では100%でなかった腰椎穿刺、アミロイド PET、FDG-PET、3T-MRI の受検率をすべて100%にするなど、バイオマーカーベースの研究が一段と進む予定である。ADNI-2 の進捗と並行して2008年から Clinical Trials of Alzheimer's Disease (CTAD) という名称の会議が開催されており、一次予防の在り方が議論されているが、これまで本邦からの参加者がいないため会議の詳細は不明である。

### III Preclinical AD の提唱

1980年代後半から90年にかけて、AD の二大プレイヤー、すなわちアミロイド蛋白(Aβ)とタウ蛋白が登場し確立された<sup>5)</sup>。この一連の研究の中で、アミロイド蛋白やタウ蛋白それぞれに対する優れた抗体が開発され、

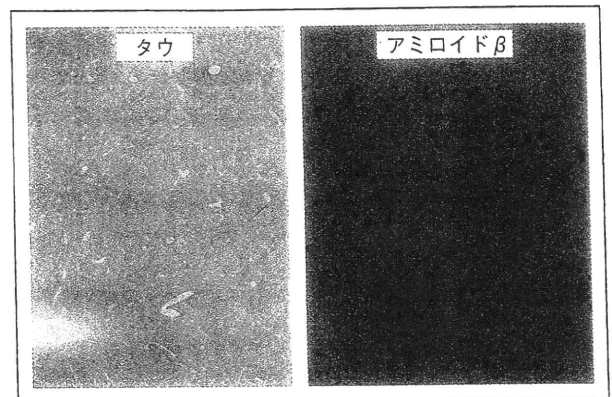


図2 Preclinical AD と考えられる病理所見

75歳非認知症高齢者の側頭葉皮質の連続切片を抗タウ抗体(左)と抗 Aβ 抗体(右)で免疫染色したもの。生前認知症症状は全くなかったが、すでに多数の Aβ 陽性の老人斑がみられるのに対してタウの変化は始まっていないことに注目(井原康夫氏原図)。

これらの抗体を用いた免疫組織染色を生前認知機能に問題はなとされていた正常者剖検脳において行ってみたところ、図2にみるような不思議な現象が観察されていた。それは、正常であるにもかかわらず、大脳皮質に多数の Aβ 陽性の老人斑が見られるが、連続する切片を抗タウ抗体で免疫組織染色しても神経原線維変化は全く見出されない。しかもこの逆、つまりタウが陽性で Aβ が陰性という AD 症例はいくら探してもみつかったこなかった(図2は井原康夫氏による)。「Aβ とタウ」この AD の二大プレイヤーの立ち位置の相互関係がつかめず多くの研究者は悩んでいたと思う(私もその1人であった)。Aβ は細胞外に蓄積した無害な埃のようなものではないかと考える研究者も少なくなかったと思う。それを理路整然と整理し、Aβ を悪玉としてすべての現象の最上流に置く考えを示したのが John Hardy と Dennis Selkoe であり、今日のアミロイド仮説の提唱となった<sup>7)</sup>。Aβ の下流にタウ、そのさらに下流に神経細胞死が位置し、最下流に認知機能障害がくるというものである。多くの研究成果がこの仮説を支持するものであったが、研究者が最も知りたいこと、すなわち「正常を逸脱し病的老化へと向かう段階で、ヒトの脳に Aβ 蛋白が蓄積してくる過程がある」ことを実証できないでいた。米国 ADNI の成果には注目すべき発見がいくつ

もあるが、その中で正常高齢者として組み入れた認知機能に全く問題のない集団において、<sup>11</sup>C-PIB アミロイド PET 陽性例や脳脊髄液 Aβ42 低値例が少なからず見出されたことは特記すべきことであろう。2008年のピッツバーグ大学の経験では正常者19名中9名が PIB 集積のカットオフ値を超えて陽性と判定されている<sup>8)</sup>。このような<sup>11</sup>C-PIB アミロイド PET 陽性例には脳脊髄液 Aβ42 低値例が多いことも明らかにされた。つまりこの2種類のバイオマーカーは、同一現象を2つの鏡に映していると考えられている。2010年のハワイにおける国際アルツハイマー病会議(ICAD)で表1のような preclinical AD の概念がはじめて提唱された<sup>9)10)</sup>。この中で、Stage 1 は、認知機能に全く問題がなくとも、アミロイド PET 陽性または脳脊髄液 Aβ42 が低値を示す場合である。正常を逸脱して AD へと向かいはじめた最初期段階と考えられる。図2の段階がおそらく Stage 1 に該当するとと思われる。ADNI ではこのような例が正常健常者として組み入れた群から少なからず見出されている。最近、Sperling らはアミロイド PET 陽性例で default network の障害を functional MRI で証明している<sup>11)</sup>。Stage 2 は、Stage 1 から10~15年経過した段階で、認知機能は正常

に保たれているが、神経細胞内ではタウ蛋白の異常リン酸化と凝集によるシナプス機能異常、さらには神経細胞死のカスケードがトリガーされた状態と解釈され、①脳脊髄液タウやリン酸化タウが高値を示す、②シナプス消失や神経細胞死を反映して糖代謝 PET (FDG-PET) において後部帯状回などで特徴的な低下を示す、③神経細胞死の全体的なマスが一定以上となると脳萎縮として MRI にて検出可能となる。しかし、いずれの段階でも標準的な認知機能検査では正常と判断される。物忘れ外来の現場ではこのような症例にまれではあるが遭遇することがある<sup>12)</sup>。Stage 3 は、以前とは違うという微細な機能低下を初めて自覚するが、MCI のレベルには至っていない段階である。

## IV 根本治療薬の治験と preclinical AD

AD において、コリンエステラーゼ阻害薬などの症状改善薬の治験は軽度から重度までの AD においておおむね成功したといえる。しかし、AD とは対照的に同様の評価法をもって MCI を対象とした治験は一部を除い

表1 米国アルツハイマー病協会から提唱されたリサーチ目的の 'preclinical AD' の診断基準

<p>Stage 1 : Aβ蓄積が始まった証拠があるが無症状の時期</p> <p>a. アミロイド PET 画像で陽性または脳脊髄液 Aβ42 が低値。</p> <p>Stage 2 : 脳アミロイドーシスに加えてシナプス機能異常や初期の神経変性が起きているが無症状の時期</p> <p>a. 脳脊髄液総タウまたはリン酸化タウが高値。</p> <p>b. FDG-PET で後部帯状回、プレクネウス、側頭・頭頂皮質で AD 様の代謝低下がある。</p> <p>c. MRI の volumetry にて、AD と同様の分布パターンで大脳皮質萎縮/灰白質の消失がみられる。</p> <p>Stage 3 : 微細な認知機能低下があるが、MCI レベルには至っていない時期</p> <p>a. 標準的な認知機能検査において、経時的な認知機能の低下が証明される。</p> <p>b. 新規に開発された認知機能検査で、微細な障害がある。</p>
---

米国ハーバード大学 Brigham and Women's Hospital の Sperling らが中心となって ICAD2010 にて公表された AD の前臨床段階 (preclinical AD) の概念。より早期の段階から Stage 1 ~ 3 までの 3 段階に分類されている。ADNI では、AD の根本治療薬の登場を目前にして、AD の診断と薬効評価パラダイムが、従来の認知機能検査ベースからバイオマーカーベースへと大きくシフトした成果といえる。